

Simulation of Biceps Femoris Musculotendon Mechanics during the Swing Phase of Sprinting

DARRYL G. THELEN¹, ELIZABETH S. CHUMANOV¹, THOMAS M. BEST¹, STEPHEN C. SWANSON², and BRYAN C. HEIDERSCHEIT¹

¹University of Wisconsin-Madison, Madison, WI; and ²The Orthopedic Specialty Hospital, Murray, UT

ABSTRACT

THELEN, D. G., E. S. CHUMANOV, T. M. BEST, S. C. SWANSON, and B. C. HEIDERSCHEIT. Simulation of Biceps Femoris Musculotendon Mechanics during the Swing Phase of Sprinting. *Med. Sci. Sports Exerc.*, Vol. 37, No. 11, pp. 1931–1938, 2005.

Introduction/Purpose: Characterization of hamstring mechanics during sprinting is fundamental to understanding musculotendon injury mechanisms. The objective of this study was to use muscle-actuated forward dynamic simulations to investigate musculotendon mechanics of the biceps femoris long head during the swing phase of sprinting. **Methods:** We used a three-dimensional linked segment model with 26 Hill-type musculotendon actuators to simulate swing phase dynamics. Muscle excitations were computed that drove the linked segment model to track measured hip and knee motion of an individual sprinting on a treadmill. The simulations were used to investigate the effect of tendon compliance on the excursions and power development of the muscle and tendinous components of the biceps femoris. **Results:** The biceps femoris musculotendon complex underwent a stretch-shortening cycle over the latter half of swing phase, with the shortening portion occurring in the final 10% of the gait cycle. Biceps femoris excitation increased markedly between 70 and 80% of the gait cycle and continued through the end of swing. Following the onset of excitation, stretch of the muscle component slowed considerably while the tendon lengthened and stored elastic energy. Simulating the sprinting movement with a more compliant tendon increased tendon elastic energy storage, thereby reducing peak muscle stretch and negative muscle work. **Conclusions:** Muscle-actuated forward dynamic simulation provides a powerful approach for investigating biomechanical factors that may contribute to the occurrence of hamstring musculotendon injuries. **Key Words:** MUSCLE INJURY, TENDON COMPLIANCE, MOTION ANALYSIS, MUSCULOSKELETAL MODELING, STRETCH-SHORTENING CYCLE, FORWARD DYNAMICS

Characterization of hamstring musculotendon mechanics during sprinting is fundamental to understanding the mechanisms of musculotendon injuries and injury patterns. It has previously been shown using kinematic musculoskeletal models that the biceps femoris long head, the most often injured hamstring muscle (16), lengthens throughout the latter half of the swing phase of sprinting, with peak stretch occurring before foot contact (35,36,39). Because the stretched hamstring muscle is also known to be active during this phase (14,33,39), the biceps femoris may be susceptible to a lengthening contraction injury during late swing (11,38).

However, limitations exist with the use of kinematic models to investigate musculotendon mechanics. In particular, the motion of the musculotendon unit is not necessarily representative of the behavior of individual muscle fibers (6,9,18). For example, ultrasound images acquired during functional human movement have shown that the gastroc-

nemius muscle fascicles can maintain an isometric length while the tendon, and hence musculotendon unit, lengthens and elastically stores energy (10). Tendon recoil during the subsequent musculotendon shortening releases the stored energy and allows the muscle fibers to shorten at slower velocities (30). It is plausible that the biarticular hamstrings exhibit similar stretch-shortening behavior during the late swing phase of sprinting, with the tendon stretching to absorb the energy associated with decelerating the leg. Tendon compliance, therefore, may act as a mechanical buffer that reduces the stretch of muscle fibers and protects against injury (12,31). Indeed, ignoring dynamic musculotendon interactions may be a factor that has contributed to other investigators estimating hamstring muscle fiber strains during sprinting (36) that exceed injury tolerances observed in animal models (5,21).

Muscle-actuated forward dynamic simulation provides a powerful framework within which to investigate musculotendon mechanics during movement. A forward dynamic model consists of a set of governing differential equations that describe activation, contraction, and skeletal dynamics (1,28). Given a set of input muscle excitations, the model can be solved to simulate the movement that would result. Thus, to the extent that the underlying equations are accurate and complete, the motion predicted by forward dynamic simulation reflects the underlying structure and properties of the musculoskeletal system. The objective of this study was to develop and use muscle-actuated forward dynamic sim-

Address for correspondence: Darryl G. Thelen, Ph.D., Department of Mechanical Engineering, University of Wisconsin-Madison, 1513 University Ave., Madison, WI 53706; E-mail: thelen@enr.wisc.edu.

Submitted for publication December 2004.

Accepted for publication June 2005.

0195-9131/05/3711-1931/0

MEDICINE & SCIENCE IN SPORTS & EXERCISE®

Copyright © 2005 by the American College of Sports Medicine

DOI: 10.1249/01.mss.0000176674.42929.de

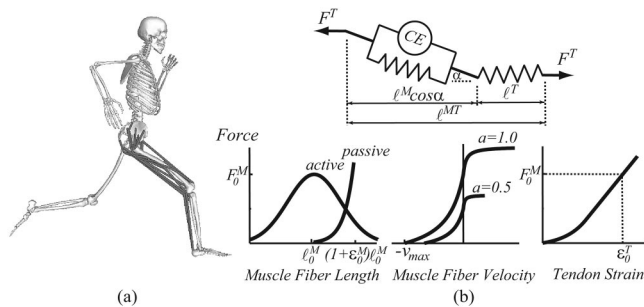


FIGURE 1—(a) Twenty-six musculoskeletal actuators were represented in the linked segment model. (b) The Hill-type model of musculoskeletal contraction dynamics included muscle force–length–velocity properties and tendon force–strain properties (40). Parameters used in the nominal simulations were: $\epsilon_0^M = 0.6$, $\epsilon_0^T = 0.05$, $v_{\max} = 5 \text{ l}_0^M/\text{s}$ (zero activation), and $v_{\max} = 15 \text{ l}_0^M/\text{s}$ (full activation). The muscle and tendon curves shown were scaled to individual muscles using four parameters (8): l_0^M , optimal fiber length; F_0^M , maximum isometric force; l_s^T , tendon slack length; and α_0 , fiber pennation angle. The parameters of the biceps femoris (BF) long head in the unscaled model were: $l_0^M = 0.109 \text{ m}$, $l_s^T = 0.341 \text{ m}$, $F_0^M = 1344 \text{ N}$, and $\alpha_0^M = 0^\circ$. The actual optimal fiber and tendon slack lengths used in subject-specific models were scaled based on measured segment lengths.

ulations to investigate biceps femoris musculoskeletal mechanics during the swing phase of sprinting. We show that a computed muscle control algorithm can be used to compute muscle excitations that accurately replicate subject-specific kinematics and are relatively consistent in timing with measured EMG activities. We demonstrate the application of the model to investigate the effects of both external (running speed) and internal (e.g., tendon compliance) factors on the muscle and tendon contributions to length excursions and mechanical work.

METHODS

Forward dynamic musculoskeletal model. Simulation of swing limb motion was performed by integrating a set of ordinary differential equations (i.e., state equations) that describe activation dynamics, musculoskeletal contraction dynamics, and the system equations of motion. The input to each muscle in the model was an idealized excitation level that could vary between zero (no excitation) and one (full excitation). Muscle activation and fiber length were the state quantities of each musculoskeletal actuator. The generalized coordinates and generalized speeds were the state variables of a linked-segment model of the human body (Fig. 1a).

The coupling of muscle excitation to activation (i.e., the process by which muscle fiber calcium concentration is modulated by motor unit action potentials) was modeled by a first-order differential equation with rise and decay time constants of 10 and 30 ms, respectively (1,40). Musculoskeletal contraction dynamics were described by a Hill-type lumped-parameter model in which a muscle contractile element is in series with an elastic tendon (40). In the model, both the muscle and tendinous components are assumed to undergo uniform deformation. A first order differential equation of contraction dynamics was used to describe the

dynamic interaction of the force–length–velocity properties of muscle and the elastic properties of tendon (Fig. 1b). In particular, at each time step, the muscle fiber velocity was computed by inverting the force–length–velocity relationship of muscle given the current activation, muscle fiber length, and the overall musculoskeletal length (32). The force produced by the musculoskeletal actuator was determined by solving for the tendon strain given the current fiber and musculoskeletal length, and then inverting the tendon–force strain relationship (Fig. 1b). Tendon forces were applied to the segments to which they were attached.

The body was modeled as a 31-*df* articulated linkage (Fig. 1a). Each hip was represented as a ball-and-socket joint with 3 *df*. The knee was modeled as a 1-*df* joint in which non-sagittal rotations and tibiofemoral translations were computed from the knee flexion–extension angle using experimentally derived functions (37). Because we were interested in hamstring musculoskeletal mechanics, only hip (flexion–extension and abduction–adduction) and knee (flexion–extension) degrees of freedom were actuated by musculoskeletal units. All other degrees of freedom were prescribed to follow measured kinematic trajectories. This allowed for intersegmental dynamics of the whole body to be properly accounted for without incorporating excessive musculoskeletal details in the model.

Twenty-six musculoskeletal actuators that cross the hip and knee were included in the model (8). The geometry of each musculoskeletal unit was described by a series of segments from origin to insertion. Wrapping surfaces were used to account for the tendinous wrapping about joints and other soft tissues (2). The normalized properties of muscle and tendon (Fig. 1) were scaled to individual muscles using four parameters: optimal fiber length, pennation angle, maximum isometric force, and tendon slack length (40).

Simulation of swing limb movement. A computed muscle control (CMC) algorithm was implemented using custom software to determine muscle excitation patterns that drove the model to replicate measurements of hip and knee angles during the swing phase of sprinting (Fig. 2). The CMC algorithm has been described in detail elsewhere (34) and is reviewed only briefly here. At a time *t* in the simulation, the difference between the simulated and experimental joint angles and angular velocities were determined. These position and velocity errors were fed back and used to compute the desired joint accelerations necessary to maintain tracking of experimental trajectories. Numerical optimization was then employed to compute a set of muscle excitations that would generate the desired accelerations while minimizing a performance criterion. Optimization was necessary because the number of muscles ($m = 26$) greatly exceeded the number of degrees of freedom ($n = 3$) being tracked, such that there were many feasible sets of muscle excitations that would generate the desired accelerations. We determined those muscle excitations that minimize the sum of muscle volume–weighted squared activations (13). A similar performance criterion has been shown to predict muscle excitation patterns that closely agree with EMG recordings and dynamic optimization solutions of

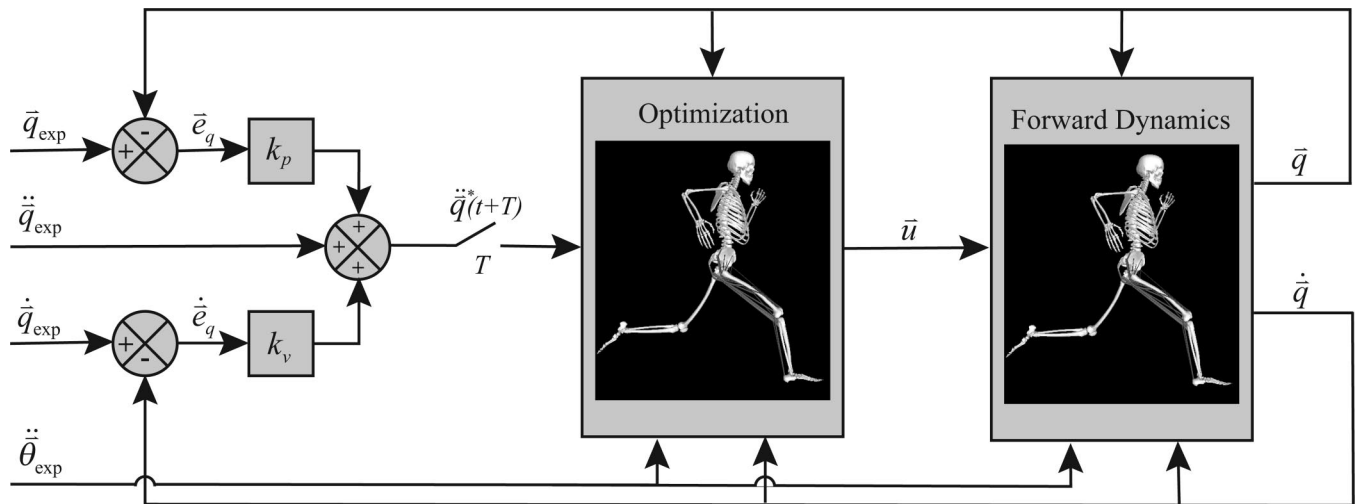


FIGURE 2—A computed muscle control algorithm was used to solve for muscle excitations (\bar{u}) that would drive the lower extremity to track measured hip and knee angles (\bar{q}_{exp}) during the swing phase of sprinting. At a time t in the simulation, errors in the joint angles (\bar{e}_q) and angular velocities ($\dot{\bar{e}}_q$) were determined and fed back to compute a desired set of accelerations (\ddot{q}^*) to achieve. Static optimization was used to solve for a set of muscle excitations that would produce the desired accelerations, while minimizing a performance criterion to resolve muscle redundancy (13). Muscle excitations were then input into the forward dynamics model and the full set of system state equations were integrated forward in time. Muscle excitations were recomputed every $T = 0.01$ s in the simulation. All other model degrees of freedom, aside from the tracked hip and knee angles, were prescribed to follow experimental trajectories ($\ddot{\theta}_{exp}$).

normal walking (1). After solving for the muscle excitations, the entire set of system state equations were integrated forward over T seconds. This process was repeated until the final time of the simulation was reached. The result was a set of time histories of simulated muscle excitations, activations, muscle lengths, musculotendon forces, and hip and knee angles and angular velocities.

Experimental data. Whole body kinematics collected while an adult male (16 yr, 68 kg, 1.75 m) sprinted on a high-speed treadmill were used to derive the forward simulations of swing phase. Representative EMG data were collected on five adult males (26.4 ± 6.7 yr, 82.7 ± 12.0 kg, 1.81 ± 0.09 m) during high-speed treadmill sprinting and used to verify the model predictions of muscle excitation timing. The kinematic data were collected at The Orthopedic Specialty Hospital in Murray, Utah, and the EMG testing was conducted at Acceleration Madison in Madison, Wisconsin. The protocols were approved by the institutional review boards of both the testing institutions and University of Wisconsin-Madison. Informed consent was obtained in accordance with institutional policy.

For both the EMG analysis and the kinematic analysis, subjects first ran at an easy running speed on a high-speed treadmill until acclimated with the experimental setup and adequately warmed up to perform maximal speed sprinting. Experimental data were then recorded at treadmill sprinting speeds ranging from 80 to 100% of the subject's maximum speed. A minimum of five strides of data were collected at each running speed.

The kinematics were measured at 200 Hz using an optical passive marker motion capture system (Motion Analysis Corporation, Santa Rosa, CA) that tracked the three-dimensional positions of 47 reflective markers placed on palpable anatomical landmarks. The linked segment model was

scaled to individual subjects using the joint-to-joint segment lengths computed from an initial calibration trial. Anthropometric properties of the segments were computed using regression equations based on subject height, body mass, and segment lengths (7). Marker kinematic data were low-pass filtered using a bidirectional fourth-order Butterworth filter with a cutoff frequency of 12 Hz. Inverse kinematic analysis, the computation of joint angles from marker kinematics, was conducted using a nonlinear global optimization algorithm. At each time step, joint angles were computed that minimized the sum of squared differences between virtual markers on the model and experimental marker kinematics.

Activity of the vastus lateralis, rectus femoris, medial hamstrings, and biceps femoris were recorded using preamplified single differential surface electrodes with a fixed interelectrode distance of 10 mm (DE-2.1, DelSys, Inc, Boston, MA). In preparation for electrode placement, the skin was cleaned with alcohol and conductive gel applied to the electrodes. Muscles of interest were identified, with the same investigator placing the electrodes for all subjects. A common ground was placed on the dorsal right wrist. Electrode cabling was secured to the subject and interfaced to an amplifier/processor unit (Bagnoli-16, DelSys, Boston, MA; CMRR >84 dB at 60 Hz; input impedance > 100 M Ω). Amplification of each channel was adjusted to maximize signal resolution, with EMG data sampled at 2000 Hz using a 12-bit A/D converter interfaced to the collection computer. Piezo-resistive footswitch signals, mounted to the heel and toe of the subject's shoes, were simultaneously recorded and used to identify foot-ground contact. The EMG data were full-wave rectified and low-pass filtered using a bidirectional low-pass Butterworth filter with a cutoff frequency of 12 Hz. Ensemble curves of the EMG data were generated

for each speed by averaging across successive strides and subjects, and then normalizing to the maximum value.

Forward dynamic simulations of the swing phase of gait were generated at sprinting speeds of 7.9, 8.4, 8.9, and 9.3 $\text{m}\cdot\text{s}^{-1}$. In addition, nominal lengths of the muscle, tendon, and musculotendon unit were computed for a relaxed (muscle excitations set to zero) upright posture. The stretch of the muscle, tendon, and musculotendon unit was then defined as the change in length relative to its length in a relaxed upright posture. The power exerted on the skeleton by the muscle (tendon) was computed as the product of the force and velocity across the muscle (tendon) component. The net work generated by the muscle and tendon components were computed by integrating the respective power curves. We separately computed work quantities for the musculotendon lengthening and shortening phases. These work quantities are hereafter referred to as the negative and positive work done by muscle and tendon, respectively. Ensemble curves of muscle stretch, force, and power development were generated for each speed by averaging across three successive strides.

Sensitivity analysis. We analyzed the effects of tendon compliance (parameterized by ϵ_0^T) on hamstring musculotendon mechanics at the fastest sprinting speed, 9.3 $\text{m}\cdot\text{s}^{-1}$. Because the biceps femoris long head is by far the most often injured of the hamstring muscles (16), all the sensitivity analyses reported in this study pertain to this muscle. Biceps femoris tendon compliance was first perturbed by ± 0.5 and $\pm 1\%$ from the nominal parameter value. In addition, we determined the effects of larger variations in BF tendon compliance on muscle stretch. This was done because of the large range of estimates for ϵ_0^T (0.03–0.09) that are reported in the literature (9,23–25,30).

For each perturbation, CMC was first used to recompute the biceps femoris muscle excitations necessary to produce the musculotendon force and length trajectories as observed in the nominal simulation. The swing phase of sprinting was then resimulated using the recomputed biceps femoris muscle excitation pattern along with the nominal muscle excitation patterns for every other muscle. In so doing, the overall movement and relative muscle loading remained consistent with the nominal simulation, albeit with altered biceps femoris musculotendon mechanics. We quantified the effect of parameter perturbations on peak muscle stretch and negative muscle work. Using the small perturbations ($<1.0\%$), a sensitivity ratio was computed by normalizing the percent change in the output to the percent change in the model parameter. The sensitivity ratios were confirmed to be highly linear for these small perturbations ($r > 0.99$).

The forward dynamic musculoskeletal model was produced using SIMM, Dynamics Pipeline (Motion Analysis Corp., Santa Rosa, CA) and SD/FAST (Parametric Technology Corporation, Waltham, MA). Optimizations within the CMC algorithm and the inverse kinematics routine were performed using a sequential quadratic programming algorithm (FSQP; AEM Design, Tucker, GA).

RESULTS

The CMC algorithm produced simulations that closely replicated experimentally recorded hip and knee angles. Mean RMS errors between experimental and model predictions were 1.2° in hip flexion–extension, 0.6° in hip abduction–adduction, and 1.5° in knee flexion–extension. The timing of computed muscle excitations compared reasonably well to EMG bursts of the major anterior and posterior thigh muscles (Fig. 3). Biceps femoris muscle excitations increased rapidly between 70 and 80% of the gait cycle, continuing through the end of swing phase.

The biceps femoris musculotendon underwent a stretch-shortening cycle during the latter half of swing phase. Peak musculotendon stretch was reached at approximately 90% of the sprinting gait cycle (Fig. 4). Stretch of the muscle component slowed considerably when the biceps femoris muscle was activated, resulting in slightly earlier occurrence of peak muscle stretch. Further, the muscle component shortened considerably less than the musculotendon unit between 80 and 90% of the gait cycle, while the tendon reached a peak stretch of 15 mm (Fig. 4). The negative work done by the musculotendon unit on the system was initially attributable to the muscle component lengthening under load. However, tendon stretch was primarily responsible for the negative work performed between 80 and 90% of the sprinting gait cycle (Fig. 4).

Sprinting speed did not substantially alter the magnitude of the estimated peak stretch of the muscle component of the biceps femoris (Fig. 5). However, the mean peak force developed by the musculotendon actuator increased considerably with speed, from 934 N at the 7.9 $\text{m}\cdot\text{s}^{-1}$ speed to 1195 N at the 9.3 $\text{m}\cdot\text{s}^{-1}$ speed.

Peak BF muscle stretch and negative muscle work both decreased with an increase in tendon compliance (Fig. 6). Increasing the tendon compliance parameter, ϵ_0^T , from 0.03 to 0.09 reduced the peak BF muscle stretch by 10 mm (Fig. 7). The negative muscle work during the musculotendon lengthening phase of swing (50–90% of gait cycle) decreased from 10.5 to 3.0 J due to increased tendon compliance.

DISCUSSION

Through the use of a CMC algorithm, we were able to determine a coordinated set of muscle excitations that drove a model to accurately track subject-specific joint kinematics during the swing phase of sprinting. The computed muscle excitations were relatively consistent in timing with experimentally measured EMG activities. The simulations were used to estimate the muscle and tendon lengths, as well as the contribution of each to musculotendon power development.

Musculotendon interactions have been the focus of several recent experimental studies. For example, the development of high sample rate ultrasound instrumentation has allowed investigators to capture gastrocnemius musculotendon behavior during functional movement (9,10,23). Interestingly, the stretch-shortening behavior predicted for the biceps femoris during the latter half of the swing phase of

sprinting in this study is qualitatively similar to that of the gastrocnemius during walking and jumping. During the stance phase of walking, the fascicles of the medial gastrocnemius remain nearly isometric while the tendon (and musculotendon unit) stretches and then recoils (10). Similarly in this study, we predict that biceps femoris muscle fiber lengthening slows considerably during late swing while the musculotendon, and hence tendon, stretches and stores energy. The tendon begins to recoil before foot contact, returning energy to the system over the final 10% of the gait cycle. Furthermore, tendon recoil reduces the subsequent muscle contraction–shortening speed such that the muscle likely consumes less ATP than if it were shortening at a higher velocity (19).

While the use of real-time ultrasound instrumentation provides a means to observe musculotendon mechanics *in vivo*, forward dynamic modeling techniques have the added advantage of facilitating parametric studies. For example, we were able to use the model to predict the effects of tendon compliance on muscle stretch and work, something that is difficult to ascertain experimentally. In our sensitivity analyses, we sought to determine the changes in fiber stretch that would occur when the overall motion and muscle loading are constant, but tendon properties are varied. When tendon compliance is varied, the tendon strain trajectory must change such that the overall force trajectory remains consistent with the nominal simulation. Tendon compliance was parameterized by the strain in the tendon, ϵ_0^T , that would occur due to the application of maximum isometric muscle force. Estimates of ϵ_0^T range from 0.03 to 0.09 depending on the muscle (9,23–25,30). Our simulations indicate that varying tendon compliance over this range substantially affects biceps femoris musculotendon interactions observed during late swing, with peak muscle stretch decreasing as tendon compliance is increased. Increasing tendon compliance also enhanced the storage of energy in the tendon, and hence reduced the amount of negative work done by the muscle.

Prior studies suggest that tendon compliance may change with fatigue and prior injury. For example, in a recent study with rabbits, series elastic compliance seemed to decrease across repeated stretch-shortening contractions, necessitating an increase in fiber stretch for the musculotendon unit to undergo the same overall excursions (6). Another investigation found that among individuals with a history of hamstring strain injuries, peak knee flexor torque occurs at a greater knee flexion angle compared with both the contralateral side and a group of noninjured subjects (4). It was suggested that the increased angle reflects a shortened optimum musculotendon length for force production, which in part may arise from the long-term presence of scar tissue at the site of prior musculotendon injury (15). This may shorten the fiber length and potentially decrease passive musculotendon compliance. Our results demonstrate that a decrease in tendon compliance in particular would necessitate larger muscle fiber stretch, assuming that the running posture is not adapted to allow the entire musculotendon complex to operate at shorter lengths. Because active fiber stretch has been shown to be a strong predictor of

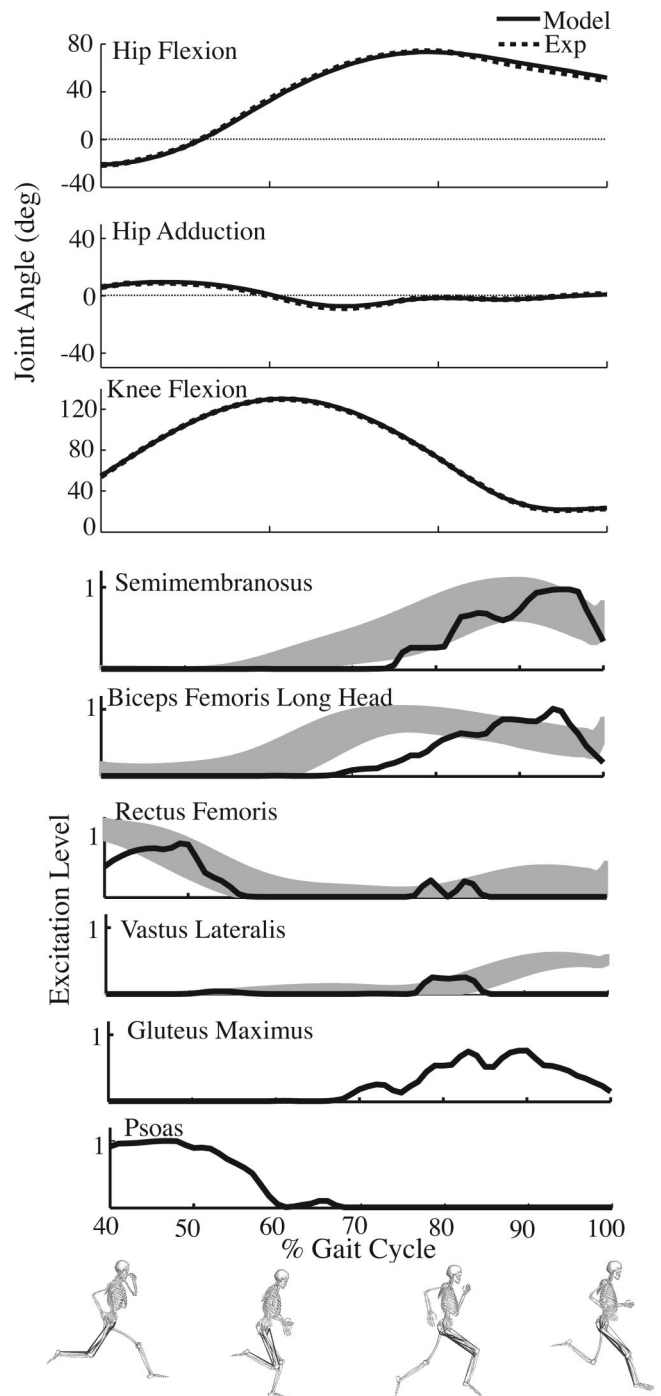


FIGURE 3—Simulation of a $9.3\text{-m}\cdot\text{s}^{-1}$ sprinting gait cycle showing that the model predicted hip and knee angles closely tracked experimental values throughout swing phase. The predicted excitations of the semitendinosus, biceps femoris, vastus lateralis, and rectus femoris are compared with measured EMG activities (shaded curves are the mean \pm 1 SD of the rectified EMG activities for five subjects). Timing of semimembranosus and rectus excitations agree closely with EMG measures. The biceps femoris excitation is slightly delayed in the simulation, though it exhibits an onset earlier than the semimembranosus as the EMG data indicate. Vastus lateralis EMG activity is most pronounced during stance (33), which was not included in our simulations of swing phase. Note that the simulations also provide excitation estimates for muscles (e.g., psoas) that cannot be monitored using surface electrodes.

lengthening contraction injury in animal models (5,20,21), an injury-induced decrease in compliance could therefore contribute

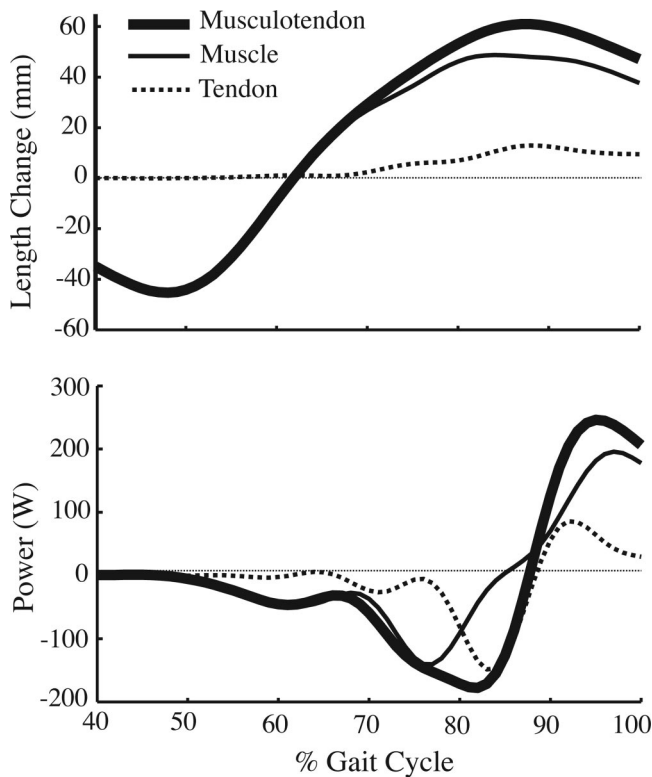


FIGURE 4—Ensemble curves (averaged over three successive strides) of the biceps femoris muscle, tendon, and musculotendon lengths, and power development during swing phase at a sprinting speed of $9.3 \text{ m}\cdot\text{s}^{-1}$. The stretch of the muscle component slows considerably when the biceps femoris is excited (starting at approximately 65% of the gait cycle), resulting in the tendon beginning to lengthen. The negative work done by the musculotendon actuator on the system is initially attributable to muscle stretch under load (50–80% of gait cycle). However, negative work done on the system between 80 and 90% of the gait cycle is due primarily to tendon stretch. The tendon recoils beyond 90% of the gait cycle, thereby returning energy to the system. Note that all length change measures are relative to corresponding lengths in a relaxed upright posture. The timing of biceps femoris muscle excitations within the gait cycle are given in Figure 3.

to the high risk of reinjury (11,27) that is seen in individuals who have previously experienced acute musculotendon injuries.

Our results also suggest that sprinting speed may have more substantial effects on muscle loading than on muscle fiber stretch. The data suggest that the load in the biceps femoris increases more substantially with sprinting speed than peak fiber stretch (Fig. 5). The increased loading is in agreement with inverse dynamics analyses of sprinting that show both the hip extensor and knee flexor moments increase with sprinting speed during late swing (17), likely due to the larger inertial loads involved in decelerating the swing leg. Assuming this load is carried by the biarticular hamstring muscles, the hamstring forces would increase with speed. Further analysis with a larger group of subjects is important to fully understand the relative speed effects on hamstring loading, work and stretch.

The musculotendon model used for this investigation was a Hill-type model, which assumes that a homogeneous tendon is connected in series with muscle fibers that undergo homogeneous strain. Some previous studies (22,23) have reported nonuniform strains along the tendon, with the apo-

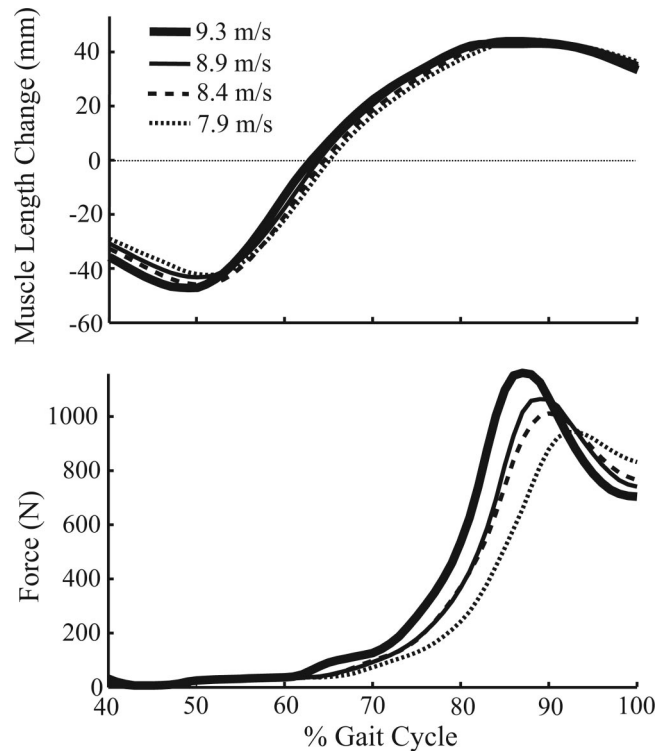


FIGURE 5—Ensemble curves of the lengthening of the biceps femoris muscle component and the force developed by the musculotendon unit across a range of sprinting speeds. The magnitude of peak muscle length change, relative to upright, is relatively independent of speed. However, the peak force developed by the musculotendon actuator increased substantially as sprinting speed was increased.

neurosis exhibiting greater compliance than the isolated tendon. In addition, imaging studies have shown that muscle strains can at times vary along the length of a fascicle (29). Given these limitations, our model predictions only allow for estimates of average strains throughout the fibers. Localized peak fiber stretch associated with injury may exceed our estimates. Future studies that can incorporate the three-dimensional musculotendon architecture (3) are needed to elucidate this finer degree of accuracy.

The musculoskeletal modeling approach used in this study has many parameters that cannot be easily measured *in vivo* on humans, and therefore must be estimated from the literature. These include muscle fiber pennation angles, optimum fiber lengths, joint articulations, and the origins and insertions of the musculotendons. These factors may contribute to the slight discrepancies between muscle excitation timing and EMG data seen in this study (Fig. 3). For example, the delay in the biceps femoris excitation onset, relative to EMG activity, could introduce some error in the musculotendon force and power predictions. As a result, there is a need for caution when interpreting the absolute results of subject-specific simulations such as those presented in this study. It is for this reason that we believe the greatest value of forward dynamic modeling lies in gaining insights into the general mechanical loading patterns and for performing detailed parameter sensitivity studies. The ability to modify single parameters within a complex system is a powerful approach to predict how performance and injury mechanics depend on specific properties of the musculoskel-

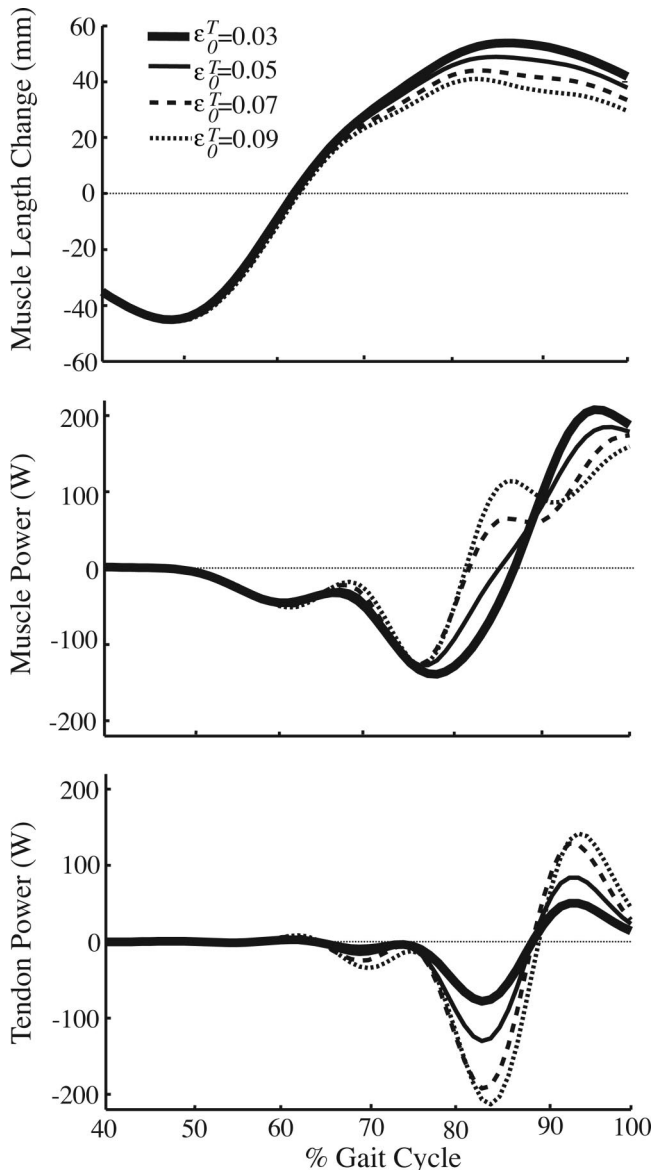


FIGURE 6—Varying tendon compliance changes the stretch and power developed by the bicep femoris muscle component during late swing phase of sprinting at $9.3 \text{ m}\cdot\text{s}^{-1}$. A less compliant tendon (lower ϵ_0^T) necessitates greater stretch and negative work to be done by the muscle component. Increasing tendon compliance (higher ϵ_0^T) reduces muscle stretch and the magnitude of negative work.

etal system. This approach has great potential for gaining insight into a variety of clinically relevant issues: for instance, the effects of changes in musculotendon properties on hamstring mechanics, and the potential of abnormal muscle timing to contribute to an acute musculotendon injury (26).

REFERENCES

- ANDERSON, F. C., and M. G. PANDY. Dynamic optimization of human walking. *J. Biomech. Eng.* 123:381–390, 2001.
- ARNOLD, A. S., S. SALINAS, D. J. ASAKAWA, and S. L. DELP. Accuracy of muscle moment arms estimated from MRI-based musculoskeletal models of the lower extremity. *Comput. Aided Surg.* 5:108–119, 2000.
- BLEMKER, S. S., P. M. PINSKY, and S. L. DELP. A 3D model of muscle reveals the causes of nonuniform strains in the biceps brachii. *J. Biomech.* 38:657–665, 2005.

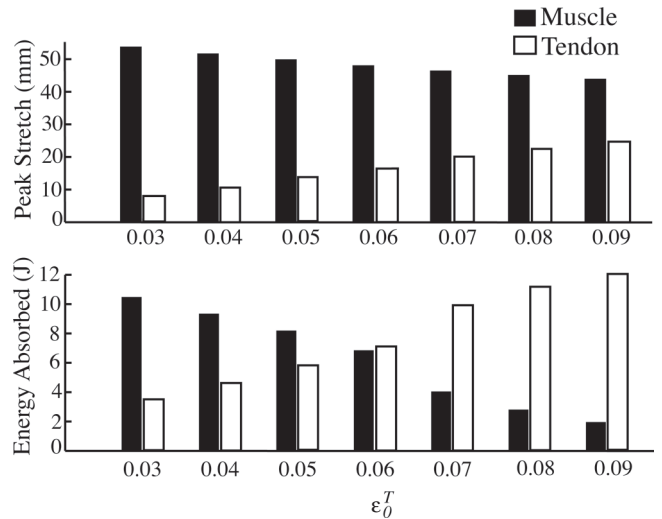


FIGURE 7—The effect of tendon compliance on the peak stretch and energy absorption of the muscle and tendon components when sprinting at $9.3 \text{ m}\cdot\text{s}^{-1}$. Peak BF muscle stretch is reduced by 10 mm as the tendon compliance parameter, ϵ_0^T , is increased from 0.03 to 0.09. A more compliant tendon absorbs more energy and reduces the negative work done by the muscle component during the musculotendon lengthening portion of the swing phase of sprinting (50–90% of gait cycle). The sensitivity (percent change in output normalized to percent change in the input) of muscle stretch and negative work is -0.17 and -0.65 for small variations about the nominal tendon compliance parameter ($\epsilon_0^T = 0.05$).

In conclusion, we have shown that it is feasible to use forward dynamic simulations to gain insights into hamstring musculotendon mechanics during the swing phase of sprinting. Our results show that tendon stretch of the biceps femoris during late swing is substantial, and acts to reduce the stretch incurred by the muscle and the amount of negative muscle work that must be done. Peak fiber stretch was found to decrease with an increase in tendon compliance, indicating the adverse injury potential that can occur due to changes in tendon mechanical properties. The use of forward dynamic simulation therefore has the potential to facilitate a more scientific approach to the understanding, prevention and treatment of musculotendon injuries.

We gratefully acknowledge the financial support provided by the Aircast Foundation and National Football League Charities, as well as a NSF Graduate Fellowship to E. Chumanov. We thank Li Li, PhD, Michael Young, Ron Kipp, and Tiffany Heath, who participated in the kinematic data collections, and Marc Schmaltz, who generously provided us access to equipment at Acceleration Madison to conduct the EMG testing. We also thank Allison Arnold, Ph.D., for the hamstring musculoskeletal models that were adapted for this study.

7. DE LEVA, P. Adjustments to Zatsiorsky-Seluyanov's segment inertia parameters. *J. Biomech.* 29:1223–1230, 1996.
8. DELP, S. L., J. P. LOAN, M. G. HOY, F. E. ZAJAC, E. L. TOPP, and J. M. ROSEN. An interactive graphics-based model of the lower extremity to study orthopaedic surgical procedures. *IEEE Trans. Biomed. Eng.* 37:757–767, 1990.
9. FUKUNAGA, T., Y. KAWAKAMI, K. KUBO, and H. KANEHISA. Muscle and tendon interaction during human movements. *Exerc. Sport Sci. Rev.* 30:106–110, 2002.
10. FUKUNAGA, T., K. KUBO, Y. KAWAKAMI, S. FUKASHIRO, H. KANEHISA, and C. N. MAGANARIS. In vivo behaviour of human muscle tendon during walking. *Proc. R. Soc. Lond. B. Biol. Sci.* 268:229–233, 2001.
11. GARRETT, W. E. JR. Muscle strain injuries. *Am. J. Sports Med.* 24:S2–8, 1996.
12. GRIFFITHS, R. I. Shortening of muscle fibres during stretch of the active cat medial gastrocnemius muscle: the role of tendon compliance. *J. Physiol.* 436:219–236, 1991.
13. HAPPEE, R. Inverse dynamic optimization including muscular dynamics, a new simulation method applied to goal directed movements. *J. Biomech.* 27:953–960, 1994.
14. JONHAGEN, S., M. O. ERICSON, G. NEMETH, and E. ERIKSSON. Amplitude and timing of electromyographic activity during sprinting. *Scand. J. Med. Sci. Sports* 6:15–21, 1996.
15. KAARIAINEN, M., T. JARVINEN, M. JARVINEN, J. RANTANEN, and H. KALIMO. Relation between myofibers and connective tissue during muscle injury repair. *Scand. J. Med. Sci. Sports* 10:332–337, 2000.
16. KOULOURIS, G., and D. CONNELL. Evaluation of the hamstring muscle complex following acute injury. *Skeletal Radiol.* 32:582–589, 2003.
17. KUITUNEN, S., P. V. KOMI, and H. KYROLAINEN. Knee and ankle joint stiffness in sprint running. *Med. Sci. Sports Exerc.* 34:166–173, 2002.
18. KUOKAWA, S., T. FUKUNAGA, A. NAGANO, and S. FUKASHIRO. Interaction between fascicles and tendinous structures during counter movement jumping investigated in vivo. *J. Appl. Physiol.* 95:2306–2314, 2003.
19. KUSHMERICK, M. J., and R. E. DAVIES. The chemical energetics of muscle contraction. II. The chemistry, efficiency and power of maximally working sartorius muscles. Appendix. Free energy and enthalpy of atp hydrolysis in the sarcoplasm. *Proc. R. Soc. Lond. B. Biol. Sci.* 174:315–353, 1969.
20. LIEBER, R. L., and J. FRIDEN. Mechanisms of muscle injury after eccentric contraction. *J. Sci. Med. Sport* 2:253–265, 1999.
21. LIEBER, R. L., and J. FRIDEN. Muscle damage is not a function of muscle force but active muscle strain. *J. Appl. Physiol.* 74:520–526, 1993.
22. LIEBER, R. L., M. E. LEONARD, C. G. BROWN, and C. L. TRESTIK. Frog semitendinosus tendon load-strain and stress-strain properties during passive loading. *Am. J. Physiol.* 261:C86–92, 1991.
23. MAGANARIS, C. N. Tensile properties of in vivo human tendinous tissue. *J. Biomech.* 35:1019–1027, 2002.
24. MAGANARIS, C. N., and J. P. PAUL. In vivo human tendon mechanical properties. *J. Physiol.* 521 Pt. 1:307–313, 1999.
25. MAGNUSSON, S. P., P. AAGAARD, P. DYHRE-POULSEN, and M. KJAER. Load-displacement properties of the human triceps surae aponeurosis in vivo. *J. Physiol.* 531:277–288, 2001.
26. ORCHARD, J. Biomechanics of muscle strain injury. *New Zealand Journal of Sports Medicine.* 30:92–98, 2002.
27. ORCHARD, J., and T. M. BEST. The management of muscle strain injuries: an early return versus the risk of recurrence. *Clin. J. Sport Med.* 12:3–5, 2002.
28. PANDY, M. G., F. E. ZAJAC, E. SIM, and W. S. LEVINE. An optimal control model for maximum-height human jumping. *J. Biomech.* 23:1185–1198, 1990.
29. PAPPAS, G. P., D. S. ASAKAWA, S. L. DELP, F. E. ZAJAC, and J. E. DRACE. Nonuniform shortening in the biceps brachii during elbow flexion. *J. Appl. Physiol.* 92:2381–2389, 2002.
30. PROSKE, U., and D. L. MORGAN. Tendon stiffness: methods of measurement and significance for the control of movement. A review. *J. Biomech.* 20:75–82, 1987.
31. REEVES, N. D., and M. V. NARICI. Behavior of human muscle fascicles during shortening and lengthening contractions in vivo. *J. Appl. Physiol.* 95:1090–1096, 2003.
32. SCHUTTE, L. M., M. M. RODGERS, F. E. ZAJAC, and R. M. GLASER. Improving the efficacy of electrical stimulation-induced leg cycle ergometry: an analysis based on a dynamic musculoskeletal model. *IEEE Trans. Rehabil. Eng.* 1:109–125, 1993.
33. SWANSON, S., and G. CALDWELL. An integrated biomechanical analysis of high speed incline and level treadmill running. *Med. Sci. Sports Exerc.* 32:1146–1155, 2000.
34. THELEN, D. G., F. C. ANDERSON, and S. L. DELP. Generating dynamic simulations of movement using computed muscle control. *J. Biomech.* 36:321–328, 2003.
35. THELEN, D. G., E. S. CHUMANOV, D. M. HOERTH, et al. Hamstring muscle kinematics during treadmill sprinting. *Med. Sci. Sports Exerc.* 37:108–114, 2005.
36. VAN DON, B. J. Hamstring injuries in sprinting. Ph.D. Dissertation. The University of Iowa, Exercise Science, Iowa City, 1998.
37. WALKER, P. S., J. S. ROVICK, and D. D. ROBERTSON. The effects of knee brace hinge design and placement on joint mechanics. *J. Biomech.* 21:965–974, 1988.
38. WHITING, W., and R. ZERNICKE. Biomechanics of Musculoskeletal Injury. Champaign, IL: Human Kinetics, 1998, 148–149.
39. WOOD, G. Biomechanical limitations to sprint running. *Med. Sci. Sports Exerc.* 25:58–71, 1987.
40. ZAJAC, F. E. Muscle and tendon: properties, models, scaling and application to biomechanics and motor control. *Crit. Rev. Biomed. Eng.* 17:359–411, 1989.